Supplementary Information for

Large Linear Magnetoelectric Effect and Field-Induced Ferromagnetism and Ferroelectricity in $DyCrO_4$

Xudong Shen,[1,2] Long Zhou,[1,2] Yisheng Chai,[3,1] Yan Wu,[4] Zhehong Liu,[1,2] Yunyu Yin,[1,2] Huibo Cao,[4] Clarina Dela Cruz,[4] Young Sun,[1,2] Changqing Jin,[1,2] Angel Muñoz,[5] José Antonio Alonso[6] & Youwen Long[1,2,7]

[1]Beijing National Laboratory for Condensed Matter Physics, Institute of Physics, Chinese Academy of Sciences, Beijing 100190, China

[2]School of Physics, University of Chinese Academy of Sciences, Beijing 100049, China

[3]Department of Applied Physics, Chongqing University, Chongqing 400044, China

[4]Neutron Scattering Division, Neutron Scattering Science Directorate, Oak Ridge National Laboratory, Oak Ridge, Tennessee 37831, USA

[5]Universidad Carlos III, Avenida Universidad 30, E-28911, Leganés-Madrid, Spain

[6]Instituto de Ciencia de Materiales de Madrid, C.S.I.C., Cantoblanco, Madrid E-28049, Spain

[7]Songshan Lake Materials Laboratory, Dongguan 523808, Guangdong, China

Correspondence: Youwen Long (ywlong@iphy.ac.cn)

Detailed analysis for neutron powder diffraction data.

1. Group theory analysis.

The crystal symmetry of the scheelite-type $DyCrO_4$ is a tetragonal $I4_1/a$ (No. 88). The neutron diffraction shows that the propagation vector is **k** = (0, 0, 0). For $I4_1/a$ space group, there are 8 irreducible representations as shown below.

	1	2_z (0,0,1/2)	4_z^+ (1/4,3/4,1/4)	4_z^- (-1/4,3/4,1/4)	$\bar{1}$ (0,1,1/2)	$\bar{2}_z$ (0,1/2,1/2)	$\bar{4}_z^+$ (-1/4,1/4,1/4)	$\bar{4}_z^-$ (1/4,1/4,1/4)
Γ_1	1	1	1	1	1	1	1	1
Γ_2	1	1	-1	-1	1	1	-1	-1
Γ_3	1	1	i	i	-1	-1	-i	-i
Γ_4	1	1	-i	-i	-1	-1	i	i
Γ_5	1	-1	1	-1	1	-1	1	-1
Γ_6	1	-1	-1	1	1	-1	-1	1
Γ_7	1	-1	i	-i	-1	1	-i	i
Γ_8	1	-1	-i	i	-1	1	i	-i

The basis vectors associated with the different irreducible representations are listed as follows. Atomic positions: Cr (1): (0, 0.25, 0.125); Cr (2): (0, 0.75, 0.375); Dy (3): (0, 0.25, 0.625); Dy (4): (0, 0.75, 0.875).

	Cr		Dy	
	(1)	(2)	(3)	(4)
Γ_1	(0,0,w)	(0,0,w)	(0,0,t)	(0,0,t)
Γ_2				
Γ_3	(u,0,0)	(u,0,0)	(r,0,0)	(r,0,0)
Γ_4	(u,0,0)	(-u,0,0)	(r,0,0)	(-r,0,0)
Γ_5				
Γ_6	(0,0,w)	(0,0,-w)	(0,0,t)	(0,0,-t)
Γ_7	(0,v,0)	(0,v,0)	(0,s,0)	(0,s,0)
Γ_8	(0,v,0)	(0,-v,0)	(0,s,0)	(0,-s,0)

2. Magnetic structure analysis at zero magnetic field.

In our neutron diffraction pattern measured at 2 K and 0 T, the most strong magnetic diffraction peak is (002). The magnetic reflection (002) is forbidden for the space group of $I4_1/a$. It implies two things: a) The magnetic moments cannot be parallel to the *c*-axis; (b) The magnetic moments of the Cr atoms (1) and (2) and Dy atoms (3) and (4) must be different. So the only possible magnetic coupling is antiferromagnetic (AFM). Therefore, the only possible magnetic structures are those corresponding to the basis vectors associated to the irreducible representations Γ_4 and Γ_8. They correspond to an AFM coupling with the moments parallel to the *a*-direction (Γ_4) or to the *b*-direction (Γ_8). As the space group is tetragonal, *a*-direction is equal to *b*-direction. Accordingly, we have tried to fit the neutron powder diffraction pattern obtained at 2 K at 0 T (see Fig. S2e). The magnetic moments we fitted for Cr^{5+} (1.0 ± 0.1 μ_B,) and Dy^{3+} (9.6 ± 0.5 μ_B) are very similar with the theoretical values. Note that these results are well in agreement with the publication (Journal of Physics: Conference Series 549, 012021, 2014).

3. Magnetic structure analysis under magnetic fields.

Firstly, we have to point out that it is difficult to fit the magnetic peaks under a magnetic field for a powder sample, because the orientation of the magnetic field with respect to the different magnetic domains. In our case, we have experimentally found the following facts. On applying a magnetic field we do not observe the appearance of new magnetic reflections or that the observed magnetic reflections disappear. It implies that the propagation vector is unchanged to be $\mathbf{k} = (0, 0, 0)$ under fields. Therefore we can only deduce that the magnetic moments become aligned along the direction of the magnetic field, inducing a canting of the moments. For a very big magnetic field all the moments would be parallel to the magnetic field and the magnetic structure would be collinear ferromagnetic (FM). We observe that the intensity of (002) reflection decreases (see Fig. S10) and it is expected that for a very high magnetic field, greater than 4.3 T we used, the intensity will be zero. On the other hand, the permitted

reflections that carry (overimposed) a magnetic reflection will increase their intensity. This is what it seems to be observed in the (011) reflection (see Fig. S10), when all the magnetic moments tend to be oriented parallel to the magnetic field. Given the polycrystalline nature of $DyCrO_4$, it is difficult to exactly determine the magnetic structure under fields (it is similar to fit a crystallographic structure with a sample with an unknown strong texture). However, we may do the following: we assume that there are two magnetic phases, the first one is the collinear AFM structure in which the moments are antiferromagnetically coupled along the *a*-direction (this is the case at 0 T); the second magnetic phase is a FM structure with all the moments parallel to the *c*-direction (this is the final arrangement that the external magnetic field will impose). We assume that the magnitudes of the magnetic moments are the same as those found at 2 K and 0 T (1.0 μ_B for Cr, 9.6 μ_B for Dy), and we only fit the scale factor. From the scale factor we can obtain a percentage of both phases as shown in Figure 4c in the manuscript.

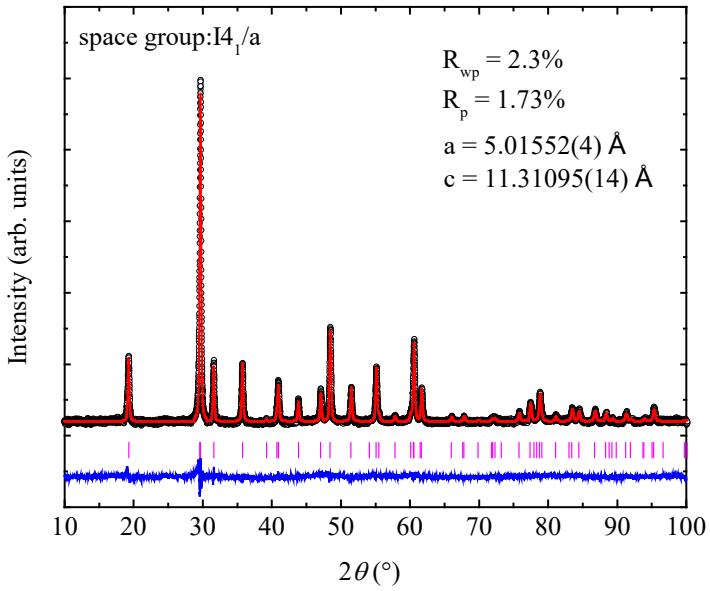

Figure S1. XRD pattern and the Rietveld refinement profiles of scheelite-type $DyCrO_4$ at room temperature. The observed (circle), calculated (red line), and difference (blue line) were shown. The magenta ticks indicate the allowed Bragg reflections.

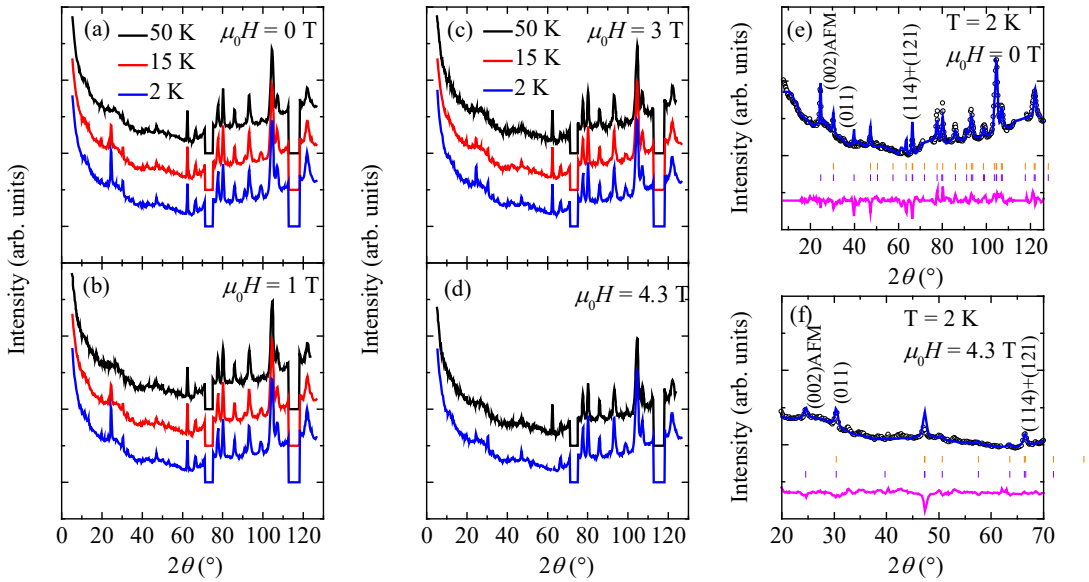

Figure S2. The NPD patterns without subtracting the nuclear contribution and the Rietveld refinement profiles of scheelite-type $DyCrO_4$. The NPD patterns measured at different temperatures and (a) μ_0H = 0 T, (b) 1 T, (c) 3 T, and (d) 4.3 T. (e, f) the Rietveld refinements for NPD data collected at 2 K and μ_0H = 0 T and 4.3 T, respectively. The observed (circle), calculated (blue line), and difference (magenta line) were shown. The top and bottom ticks indicate the allowed Bragg reflections for nuclear and magnetic reflections, respectively. In (e), the R_{Bragg} = 13.3% for both nuclear and magnetic diffractions. In (f), the R_{Bragg} = 14.2% for nuclear and 32.3% for magnetic. As we mentioned in the manuscript, for polycrystalline sample, it is difficult to exactly fit the magnetic peaks collected under a magnetic field, because of the orientation of magnetic field with respect to different magnetic domains. This is the reason for the high R_{Bragg} for magnetic in (f). However, the magnetic structure we proposed is no problem, as no new peaks appear and it is only observed a change in the intensity. In particular the intensity of the (002) reflection, whose nuclear contribution is zero and it is only magnetic (associated to the AFM ordering), decreases on increasing the value of the magnetic field. Note that we have considered only the six magnetic reflections that are more importants for magnetic refinments in (e) and (f).

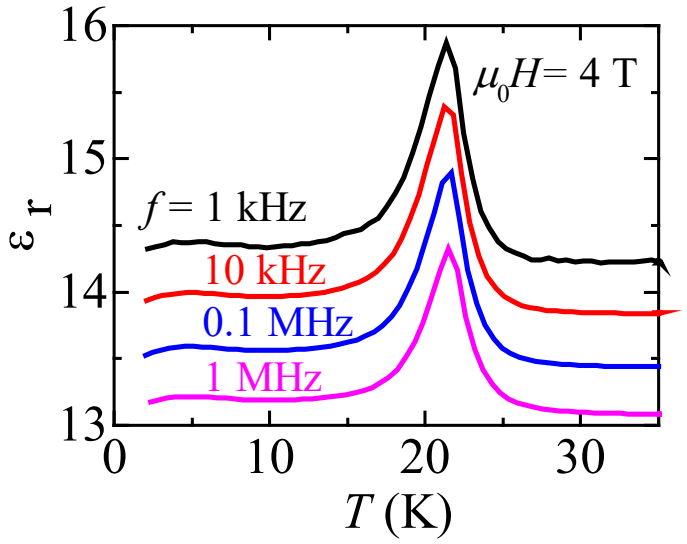

Figure S3. Temperature dependence of relative dielectric constant ε_r measured at 4 T using different frequencies. For clarity, the data were shifted in equal space along the *y*-axis.

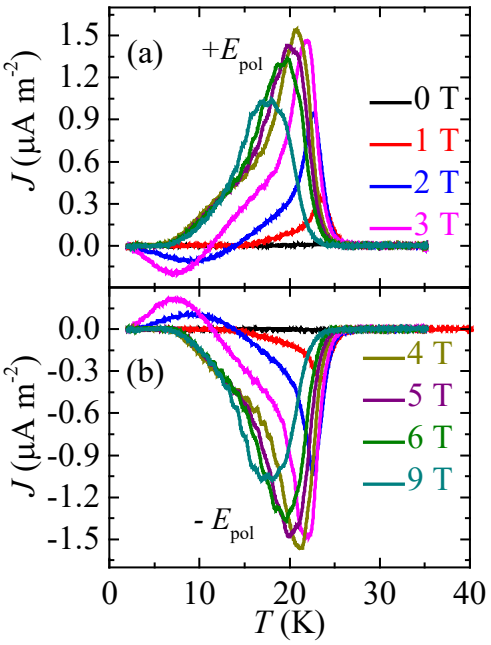

Figure S4. Temperature dependence of pyroelectric current density J related to Figure 1e,f in main text after poling under different magnetic fields with poling electric field E_{pol} (a) = 1.08 MV m^{-1}, and (b) = -1.08 MV m^{-1}.

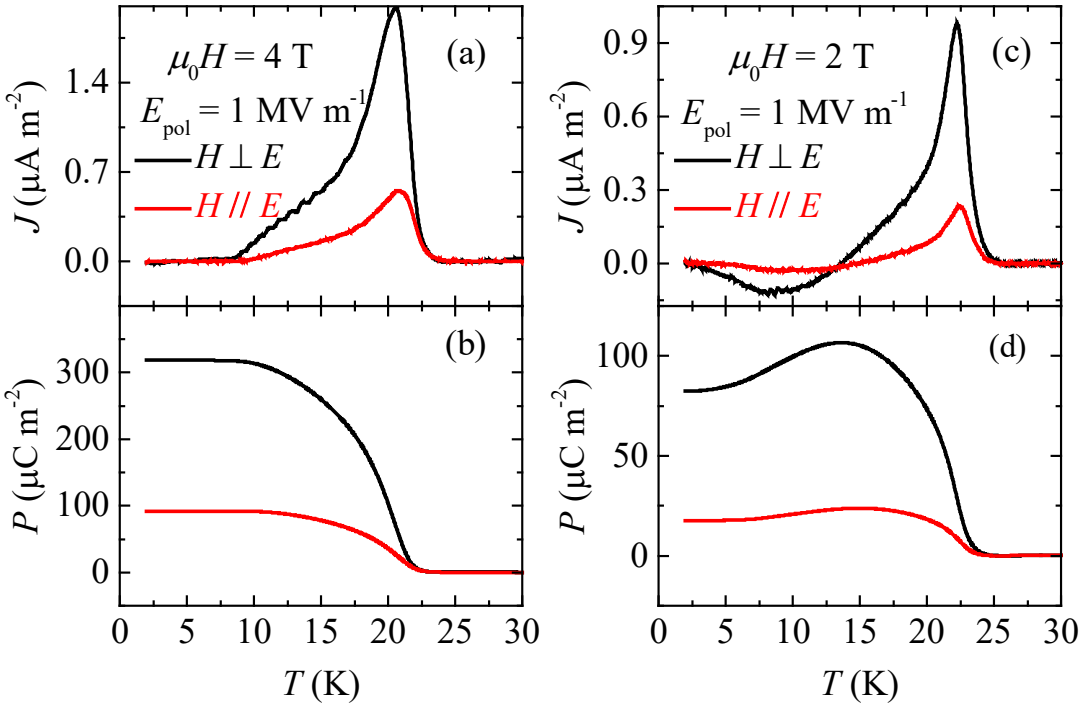

Figure S5. Temperature dependence of pyroelectric current density J and electric polarization P measuted $H // E$ and $H \perp E$. (a, b) Temperature dependent J and related P at $\mu_0 H = 4$ T . (c, d) Temperature dependent J and related P at $\mu_0 H = 2$ T . The P were determined from the integration of J with respect to time.

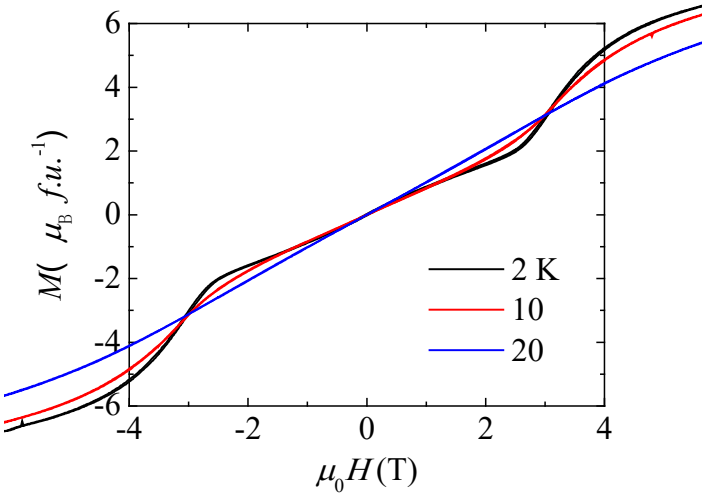

Figure S6. Magnetization as a function of applied magnetic field ranging from -4 to 4 T below T_N.

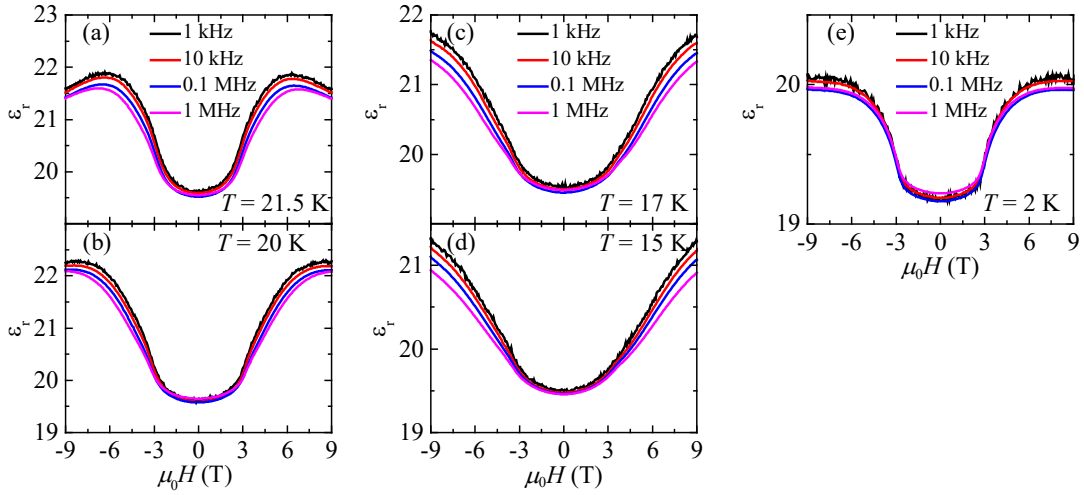

Figure S7. The relative dielectric constant as a funtion of external magnetic field at different frequencies and (a) T = 21.5 K, (b) 20 K, (c) 17 K, (d) 15 K, (e) 2 K.

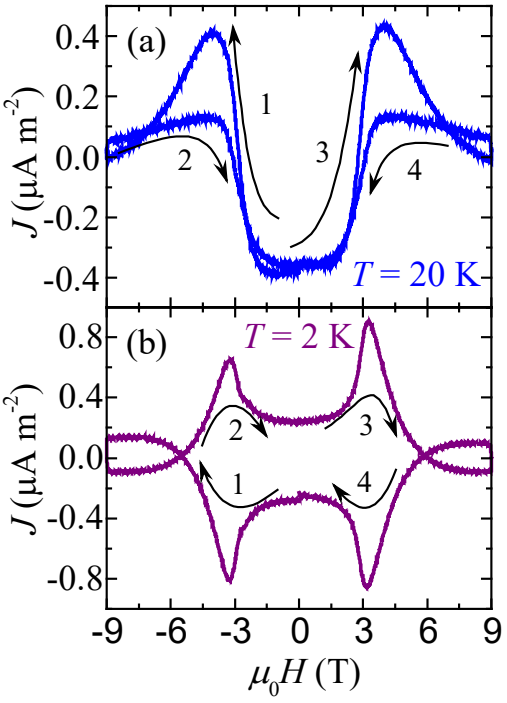

Figure S8. The magnetoelectric current density J as a function of magnetic field related to Figure 2c,e in the main text at (a) T = 20 K, and (b) 2 K. The scan sequences of magnetic field are indicated by the arrows and numbers.

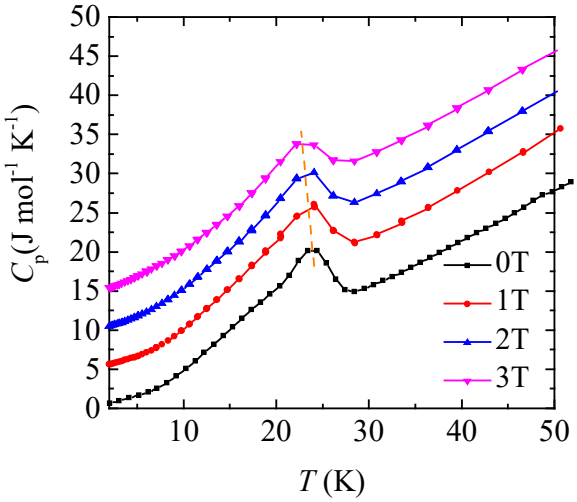

Figure S9. Temperature dependent specific heat C_p of scheelite-type $DyCrO_4$ measured at different magnetic fields. For clarity, the data were shifted in equal space along the *y*-axis.

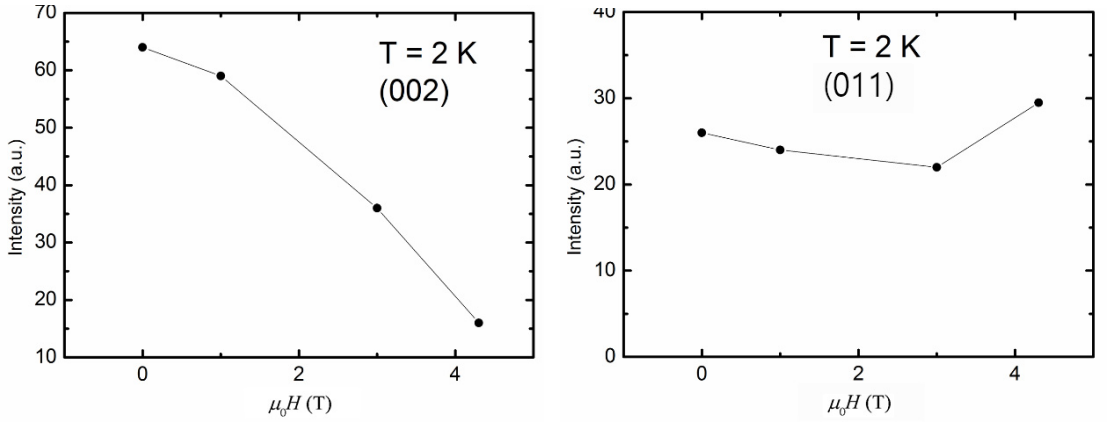

Figure S10. Magnetic field dependence of the magnetic (002) and (011) reflections at 2 K in $DyCrO_4$.